Article
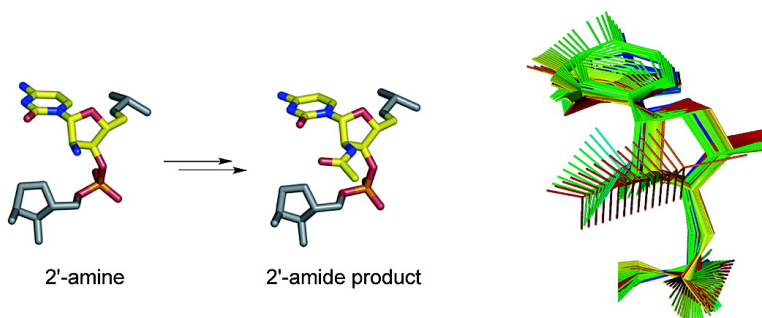
Crystal Structures, Reactivity and Inferred Acylation Transition States for 2'-Amine Substituted RNA

Costin M. Gherghe, Joseph M. Krahn, and Kevin M. Weeks

2'-amine   2'-amide product

More About This Article

Additional resources and features associated with this article are available within the HTML version:

- Supporting Information
- Links to the 4 articles that cite this article, as of the time of this article download
- Access to high resolution figures
- Links to articles and content related to this article
- Copyright permission to reproduce figures and/or text from this article

View the Full Text HTML

Crystal Structures, Reactivity and Inferred Acylation Transition States for 2′-Amine Substituted RNA

Costin M. Gherghe, Joseph M. Krahn,[†] and Kevin M. Weeks*

Contribution from the Department of Chemistry, University of North Carolina, Chapel Hill, North Carolina 27599-3290

Received June 3, 2005; E-mail: weeks@unc.edu

Abstract: Ribose 2′-amine substitutions are broadly useful as structural probes in nucleic acids. In addition, structure-selective chemical reaction at 2′-amine groups is a robust technology for interrogating local nucleotide flexibility and conformational changes in RNA and DNA. We analyzed crystal structures for several RNA duplexes containing 2′-amino cytidine (C^N) residues that form either C^N–G base pairs or C^N–A mismatches. The 2′-amine substitution is readily accommodated in an A-form RNA helix and thus differs from the C2′-endo conformation observed for free nucleosides. The 2′-amide product structure was visualized directly by acylating a C^N–A mismatch in intact crystals and is also compatible with A-form geometry. To visualize conformations able to facilitate formation of the amide-forming transition state, in which the amine nucleophile carries a positive partial charge, we analyzed crystals of the C^N–A duplex at pH 5, where the 2′-amine is protonated. The protonated amine moves to form a strong electrostatic interaction with the 3′-phosphodiester. Taken together with solution-phase experiments, 2′-amine acylation is likely facilitated by either of two transition states, both involving precise positioning of the adjacent 3′-phosphodiester group.

Introduction

RNA molecules fold into diverse three-dimensional shapes and interact with proteins and other ligands in idiosyncratic ways. Many RNA tertiary interactions and intermolecular interactions with ligands are mediated by or lie near the ribose 2′-hydroxyl group. One extremely useful probe for analyzing RNA structure and RNA-ligand interactions has therefore been to substitute the 2′-OH group with a 2′-amine.[1,2] The 2′-amine substitution is broadly useful (i) as an intrinsic functional group probe for interactions at the 2′-OH,[3–5] (ii) as a selective nucleophilic handle for introducing site-specific cross-linking[1,6] or fluorescent probes,[7,8] and (iii) for conferring nuclease resistance to an RNA.[9] 2′-Amine chemistry also inspired the substrate-assisted catalysis model for peptide bond formation on the ribosome,[10] that has recently been corroborated in biochemical work.[11]

Substitution of a 2′-amine for the 2′-hydroxyl is a conservative, but not silent, change in RNA. A 2′-amine has a pK_a of ~6 [10,12] and thus exists in the $-NH_2$ form at neutral or higher pH. Like the 2′-OH, a 2′-NH_2 group can function both as a hydrogen bond acceptor and donor. However, the more basic $-NH_2$ group is likely a better H-bond acceptor, but weaker H-bond donor than the 2′-OH. In isolated nucleosides, the 2′-amine substituted ribose favors the C2′-endo (DNA-like) ring conformation, but the barrier for conversion to the C3′-endo (RNA-like) conformation appears to be small.[13] The 2′-amine substitution modestly destabilizes nucleic acid duplexes,[5,12,14] but can be stabilizing in other contexts.[3] RNAs containing 2′-amine substituted nucleotides are good substrates for reverse transcriptase enzymes[15,16] and 2′-amino nucleoside triphosphates are substrates for phage RNA polymerases, although these polymerases strongly prefer unmodified nucleotides.[15,17,18]

Selective reaction at 2′-amine substituted nucleotides also forms the basis for a new nucleic acid technology. Chemical reactivity at a 2′-amine substituted nucleotide is exquisitely sensitive to local nucleotide flexibility in both RNA and DNA (Figure 1).[8,10,14–16,19] Reaction at a 2′-amine to form an

† Laboratory of Structural Biology, NIEHS, National Institutes of Health, Research Triangle Park, NC 27709.

(1) Earnshaw, D.; Gait, M. *Biopolymers* **1998**, *48*, 39–55.
(2) Verma, S.; Eckstein, F. *Annu. Rev. Biochem.* **1998**, *67*, 99–134.
(3) Williams, D. J.; Boots, J. L.; Hall, K. B. *RNA* **2001**, *7*, 44–53.
(4) Pieken, W. A.; Olsen, D. B.; Benseler, F.; Aurup, H.; Eckstein, F. *Science* **1991**, *253*, 314–317.
(5) Narlikar, G. J.; Khosla, M.; Usman, N.; Herschlag, D. *Biochemistry* **1997**, *36*, 2465–2477.
(6) (a) Sigurdsson, S. T.; Tuschl, T.; Eckstein, F. *RNA* **1995**, *1*, 575–583. (b) Cohen, S. B.; Cech, T. R. *J. Am. Chem. Soc.* **1997**, *119*, 6259–6268. (c) Stage-Zimmermann, T. K.; Uhlenbeck, O. C. *Nat. Struct. Biol.* **2001**, *8*, 863–867. (d) Buchmueller, K. L.; Hill, B. T.; Platz, M. S.; Weeks, K. M. *J. Am. Chem. Soc.* **2003**, *125*, 10850–10861.
(7) (a) Silverman, S. K.; Cech, T. R. *Biochemistry* **1999**, *38*, 14224–14237. (b) Merino, E. J.; Weeks, K. M. *J. Am. Chem. Soc.* **2005**, *127*, in press.
(8) Merino, E. J.; Weeks, K. M. *J. Am. Chem. Soc.* **2003**, *125*, 12370–12371.
(9) Olsen, D. B.; Benseler, F.; Aurup, H.; Pieken, W. A.; Eckstein, F. *Biochemistry* **1991**, *30*, 9735–9741.

(10) Chamberlin, S. I.; Merino, E. J.; Weeks, K. M. *Proc. Natl. Acad. Sci. U.S.A.* **2002**, *99*, 14688–14693.
(11) Weinger, J. S.; Parnell, K. M.; Dorner, S.; Green, R.; Strobel, S. A. *Nat. Struct. Mol. Biol.* **2004**, *11*, 1101–1106.
(12) Aurup, H.; Tuschl, T.; Benseler, F.; Ludwig, J.; Eckstein, F. *Nucl. Acids Res.* **1994**, *22*, 20–24.
(13) Guschlbauer, W.; Jankowski, K. *Nucl. Acids Res.* **1980**, *8*, 1421–1433.
(14) John, D. M.; Weeks, K. M. *Biochemistry* **2002**, *41*, 6866–6874.
(15) Chamberlin, S. I.; Weeks, K. M. *J. Am. Chem. Soc.* **2000**, *122*, 216–224.
(16) Chamberlin, S. I.; Weeks, K. M. *Biochemistry* **2003**, *42*, 901–909.
(17) Aurup, H.; Williams, D. M.; Eckstein, F. *Biochemistry* **1992**, *31*, 9636–9641.
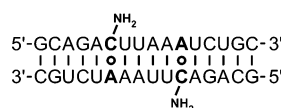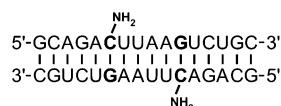(18) Padilla, R.; Sousa, R. *Nucl. Acids Res.* **1999**, *27*, 1561–1563.
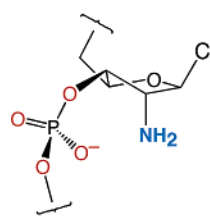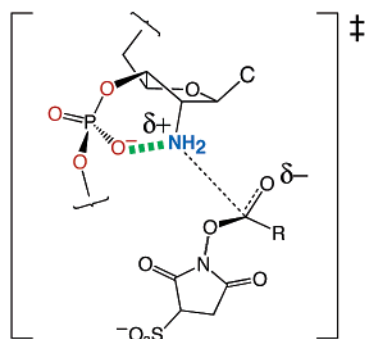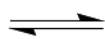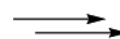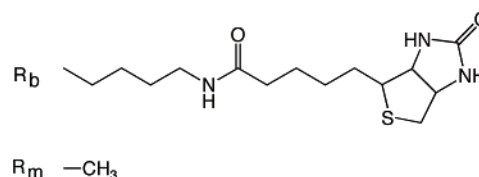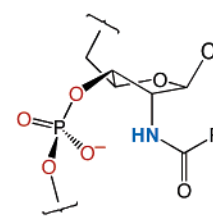
Figure 1. 2′-Amine acylation is gated by local nucleotide flexibility. Flexible 2′-amine substituted nucleotides react preferentially with an activated (succinimidyl) ester to yield the 2′-amide product because they more readily adopt a conformation that stabilizes (green dashed line) the acylation transition state. Two ester R-groups are used in this work, a bulky biotinamido group (R_b) for solution-phase chemistry and a methyl group (R_m) for in-crystal reactions.

amide[10,14,15,19] or pyrrolinone ring[8] involves significant bond formation at the amine nucleophile in the transition state and thus transient formation of a large partial positive charge on nitrogen (Figure 1). This transition state can be stabilized by proper positioning of an adjacent 3′-phosphodiester group.[10,20] This structure-sensitive chemical reaction at a 2′-amine is strongly correlated with local nucleotide flexibility because unconstrained nucleotides are better able to reach the more reactive transition state, involving an unusual local conformation (Figure 1).

We sought to understand the structural consequences of introducing a 2′-amine substitution into RNA and to place constraints on the conformation of the facilitated 2′-amine acylation transition state. We report four crystal structures for RNA duplexes containing 2′-amino cytidine (C^N) nucleotides. Analysis of these structures indicates that, in contrast to the observation for free nucleosides,[13] 2′-amine substituted nucleotides are easily accommodated in the C3′-endo (RNA-like) ribose geometry, without distorting an A-form helix, both as canonical C^N–G pairs and as C^N–A$^+$ (protonated A) mismatches.

We also show that flexible, mispaired 2′-amine substituted nucleotides can be acylated in intact crystals and the resulting 2′-amide product (see Figure 1) does not significantly perturb the duplex structure. The 2′-amine acylation transition state, in which the amine carries a large partial positive charge, was visualized in an approximate way by solving the structure of a duplex containing protonated ($-NH_3^+$) amine groups. These structures, together with solution-phase biochemical experiments, support a trajectory[21] for structure-selective 2′-amine acylation in which facilitated transition states are formed via two distinct local nucleotide conformations.

(19) (a) John, D. M.; Merino, E. J.; Weeks, K. M. *J. Mol. Biol.* **2004**, *337*, 611−619. (b) John, D. M.; Weeks, K. M. *Chem. Biol.* **2000**, *7*, 405−410.
(20) Merino, E. J.; Wilkinson, K. A.; Coughlan, J. L.; Weeks, K. M. *J. Am. Chem. Soc.* **2005**, *127*, 4223−4231.

Figure 2. C^N−A and C^N−G self-complementary duplexes. There is a single 2′-amine substitution per strand, at position 6 (C^N).

Results

Structural Overview. We have solved the structures of four self-complementary 16 base pair RNA duplexes containing a 2′-amine substitution at position 6 (Figure 2) at resolutions ranging from 2.1 to 3.2 Å. The duplexes were designed such that the unique 2′-amino cytidine nucleotide in each strand forms either a C^N−A mismatch or canonical C^N−G pair (Figure 2). The four structures include C^N−A and C^N−G *duplexes* at pH 8; a 2′-amide *product* structure, obtained by treating an intact C^N−A duplex crystal with a succinimidyl ester; and a structure of the C^N−A duplex at pH 5, where the 2′-amine group is protonated. An additional *control* duplex containing all 2′-hydroxyl groups was solved at 2.1 Å resolution. All five structures crystallized in the same space group and with similar unit cell dimensions (Table 1).

The RNA duplexes stack end-to-end in the crystal to form pseudo-infinite helices parallel to the crystallographic *c* axis

(21) A movie (in QuickTime format) illustrating plausible trajectories for the 2′-amine acylation reaction is provided in the Supporting Information. Trajectories are illustrated for facilitated transition states that proceed via both (*i*) local backbone movement and (*ii*) rotation of the substrate nucleotide into the minor groove.

Table 1. Crystal Statistics and Refinement Parameters

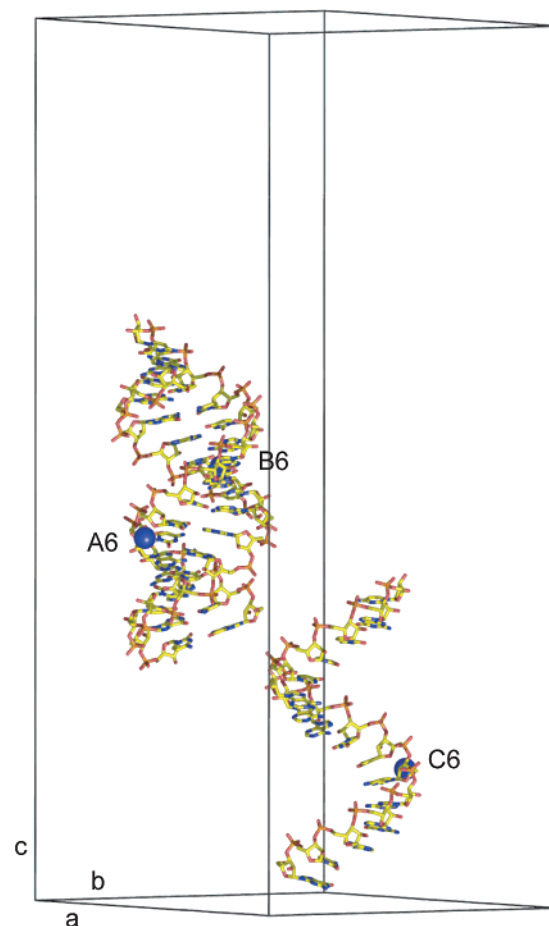|	C^N–A (pH 8)	C^N–A (pH 5)	C^N–G	C^N–A amide product	C–A control
		A. Crystal Statistics			
space group	$P3_121$	$P3_121$	$P3_121$	$P3_121$	$P3_121$
cell parameters					
$a = b$ (Å)	43.0	43.0	43.0	42.6	43.0
c (Å)	122.5	122.0	121.0	121.0	122.0
resolution (Å)	2.4	2.5	2.18	2.9	1.98
unique reflections	5305	4904	6646	3450	8972
completeness (%)	95.2	98.6	91.4	97.8	93.8
R-merge (%)	4.4	8.0	7.7	15.0	8.3
		B. Refinement			
reflections used	4649	4436	5556	2217	7927
resolution range	8.0–2.5	8.0–2.55	8.0–2.35	9.0–3.2	19–2.1
R_{work}/R_{free}	23.4/27.8	21.7/26.2	23.6/29.2	23.2/26.4	26.1/28.0
rms deviation					
bonds	0.005	0.005	0.005	0.006	0.004
angles	0.9	0.9	0.9	1.2	0.9
PDB ID	1YRM	1Z79	1YZD	1YY0	1Z7F

(Figure 3). Lateral interactions between helices are mediated by a small number of interactions between ribose 2′-hydroxyl groups. All ribose conformations are C3′-endo, as expected for A-form RNA. Superposition of the duplex structures with canonical A-form RNA gives root-mean-square deviations of 1.78 Å for the C^N–A duplex at pH 8, 1.79 Å for the C^N–A duplex at pH 5, and 1.58 Å for the C^N–G duplex.

The asymmetric unit contains three RNA strands comprising one full duplex and one single strand "wrapped" around the *c* axis (Figure 3). The complement for the third strand is provided by a symmetry-partner in the unit cell; the complete unit cell contains 9 full duplexes. There are thus three independent 2′-amine substituted cytidine residues in the asymmetric unit, each of which can be analyzed independently (Figure 3).

C^N–A and C^N–G Pairs at pH 8. Structures for each of the three C^N–A mismatches and the C^N–G base pairs are well defined by the experimental electron density (Figure 4C). None of the three 2′-amine groups makes an intermolecular interaction in the crystals. The 2′-amine at position A6 has the largest surrounding solvent pocket; however, all 2′-amine groups are at least 4.5 Å distant from other non-hydrogen RNA atoms in the crystal. Superposition of the three independent C^N–A or C^N–G pairs shows that the local geometries at each pair are very similar and independent of the local crystal environment (Figure 4A,B).

In the C^N–A mismatch (Figure 4A), the adenosine N1 and cytidine O2 atoms are, on average, 2.64 Å apart, consistent with the formation of a strong hydrogen bond between these positions. Hydrogen bond formation implies that the adenosine N1 is protonated, even at pH 8, as observed for unmodified all-ribose C–A mismatches.[22,23] The second hydrogen bond in the C^N–A^+ mismatch, between the adenine N6 and cytidine N3 at 3.04 Å, is actually slightly less intimate than the one requiring protonation of N1 (Figure 4A).

The C^N–G base pair (Figure 4B) forms, as expected, the three strong hydrogen bonds typical of the canonical base pair. The C^N–A and C^N–G pairs superimpose almost perfectly with pairs lacking the 2′-amine substitution, indicating that the 2′-ribose

(22) Pan, B.; Mitra, S. N.; Sundaralingam, M. *J. Mol. Biol.* **1998**, *283*, 977–984.
(23) Jang, S. B.; Hung, L. W.; Chi, Y. I.; Holbrook, E. L.; Carter, R. J.; Holbrook, S. R. *Biochemistry* **1998**, *37*, 11726–11731.

Figure 3. RNA duplex crystal asymmetric unit in the $P3_121$ space group. 2′-Amine substitutions are emphasized as blue spheres. The asymmetric unit contains three unique 2′-amine groups.
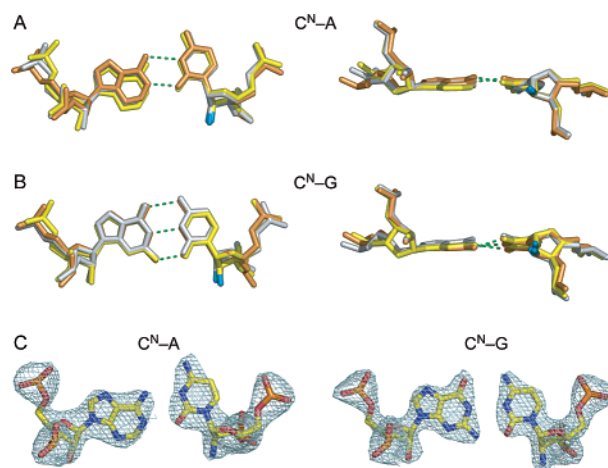
Figure 4. Conserved structure at the (A) C^N–A and (B) C^N–G base pairs at pH 8. The 2′-amine group is blue. Base pairs involving nucleotides A6, B6, and C6 are shown in orange, gray and yellow, respectively. (C) Representative electron density, contoured at 1σ, for the C^N–A mismatch and C^N–G base pair at position C6.

substitution has no significant consequence for local RNA duplex structure (not shown).

Solution Phase Selective 2′-Amine Acylation. 2′-amine substitutions in RNA react with electrophilic reagents in a reaction that is strongly gated by the underlying local nucleotide flexibility[8,10,14,16,19] (Figure 1). There is a strong correlation between the number and the quality of hydrogen bonds formed

Table 2. Crystallization Conditions[a]

C^N−A Duplex, pH 8	15% MPD, 50 mM Na-cacodylate (pH 8.0), 12 mM spermidine, 80 mM SrCl$_2$
C^N−A Duplex, pH 5	15% MPD, 100 mM Na-cacodylate (pH 5.0), 12 mM spermine, 80 mM CaCl$_2$, (net pH 5.2)
C^N−G Duplex	10% MPD, 40 mM Hepes (pH 8.0), 12 mM spermine, 80 mM MgCl$_2$, 80 mM CaCl$_2$
C^N−A Amide Product	10% MPD, 50 mM Na-cacodylate (pH 8.0), 12 mM spermidine, 80 mM CaCl$_2$
C−A Control Duplex	10% MPD, 40 mM Na-cacodylate (pH 7.0), 12 mM spermine, 80 mM SrCl$_2$, 80 mM MgCl$_2$

[a] Solutions were equilibrated against a reservoir containing 35% (v/v) MPD.
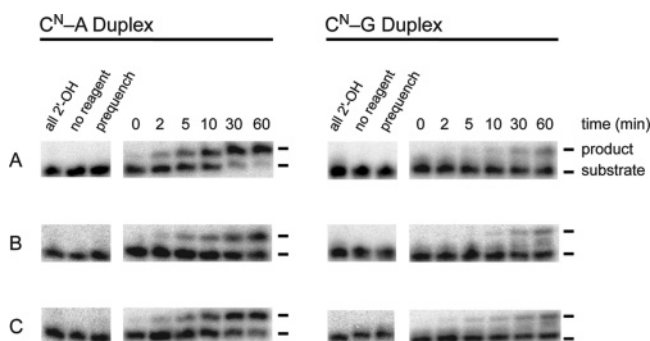
Figure 5. Solution phase 2'-amine acylation. 2'-acylated products were resolved from 2'-amine substrate duplexes as low mobility species by denaturing gel electrophoresis. Panels differ only in the solution conditions: (A) 100 mM Hepes (pH 8.0); (B) under C^N−A duplex (pH 8.0) crystallization conditions (see Table 2); (C) under C^N−A duplex (pH 8.0) crystallization conditions without spermidine. Prequench and all 2'-OH lanes indicate reactions in which the DTT quench was added prior to the succinimidyl ester reagent or in which the 2'-amine is replaced by a 2'-hydroxyl, respectively. 2'-amine acylation rates (k_{acyl}, min^{-1}) for C^N−A and C^N−G are, respectively: (A) 0.077 and 0.008. (B) 0.018 and 0.006. (C) 0.051 and 0.014.

in a base pair and the 2'-amine acylation reaction rate.[14] We therefore tested 2'-amine reactivity for each duplex, both under the standard conditions previously used to explore 2'-amine chemistry (100 mM Hepes, pH 8)[14] and under the conditions used to obtain the C^N−A duplex crystal at pH 8 (Table 2).

The bulky 2'-amide product, formed from the biotin-linked ester (R$_b$, see Figure 1), is readily resolved from the free 2'-amine substrate oligonucleotide by denaturing gel electrophoresis (Figure 5). In the simple Hepes buffer, the 2'-amine substituted cytidine in the C^N−A mismatch reacts 10-fold faster than in the C^N−G duplex (Figure 5A). Acylation of the C^N−A duplex is efficient and 90% of the RNA reacts to form the 2'-amide product over 60 min. Reaction is selective for the 2'-amine position because no acylated product is observed when the nucleophilic 2'-amine is replaced by a 2'-OH (see all 2'-OH lanes in Figure 5).

We determined acylation rates for the C^N−A duplex under conditions used for crystallization, both in the presence and absence of spermidine ions (because the polyamine reacts with and partially quenches the succinimidyl ester). Under either set of conditions, the C^N−A mismatch reacts 3 to 4-fold faster than the C^N−G duplex (Figure 5B,C). The moderately reduced absolute reactivity observed for the C^N−A mismatch, relative to that in the simpler Hepes buffer, reflects the high concentration of divalent ions used in the crystallization experiment and yields reduced local nucleotide flexibility at the mismatch.
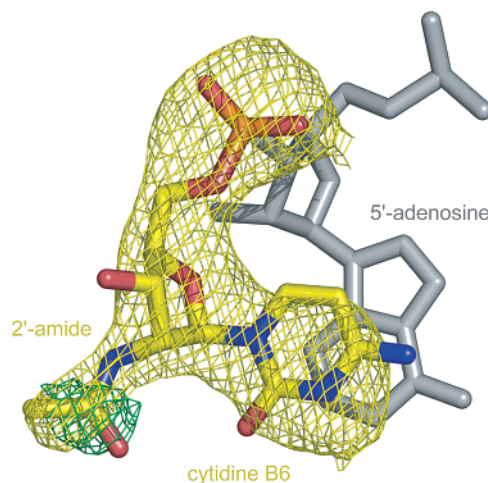
Figure 6. Refinement of the 2'-amide product, obtained by in-crystal acylation of the C^N−A mismatch duplex. Positive density observed in a $|F_o| - |F_c|$ map calculated after a single round of refinement, contoured at 2.5σ, is green. A simulated annealing omit map[28] calculated at 1.5σ is yellow; the 2'-amine substituted cytidine nucleotide and 2'-amide product atoms were excluded in this calculation.

The conditions used for crystallization thus reproduce the key mechanistic feature of 2'-amine chemistry. 2'-amine substitutions at flexible, mismatched nucleotides more readily react to form the 2'-amide product (Figure 5B,C).

2'-Amine Acylation in an Intact Crystal. We visualized the 2'-amide product directly by treating C^N−A duplex crystals with an activated ester. The simpler sulfosuccinimidyl acetate (R$_m$, Figure 1) replaced the bulkier biotin-linked ester, used in the solution phase experiments, to facilitate reagent diffusion into the crystal. After a single round of refinement, a simple $|F_o| - |F_c|$ difference map, contoured at 2.5σ, indicated that in-crystal 2'-amine acylation occurred at a single site in the asymmetric unit, at position B6 (green density in Figure 6).

A simulated annealing omit map from the final crystallographic refinement shows that atoms corresponding to the 2'-amide product are defined by the experimental electron density at a confidence level comparable to that for the cytosine base and ribose atoms (yellow density, Figure 6). The 2'-amide product does not perturb the local architecture at the RNA backbone (Figure 7A) and forms readily, in part, because it lies in a large solvent-accessible channel in the crystal (Figure 7B). The C^N−A base pair is also unperturbed and the 2'-amide nucleotide remains in the C3'-endo conformation.

In sum, neither the original 2'-amine substitution, nor formation of the 2'-amide product significantly perturbs the structure of an RNA duplex. We conclude that the 2'-amine substrate and product ground states for the 2'-amine acylation reaction are very similar and differences in these structures do not provide an adequate explanation for the exquisite sensitivity of 2'-amine acylation to local nucleotide flexibility.[10,14,15]

C^N−A Duplex at pH 5 as a Transition State Analogue. In an amide-forming transition state, a large partial positive charge forms on the amine nucleophile (Figure 1). An approximate view of this partial positive charge in the transition state can be obtained by protonating a free 2'-amine. The pK_a of a 2'-amine in RNA is 6.0−6.5.[10,12] Therefore, we solved the structure of the C^N−A duplex at pH 5.2 (Tables 1 and 2) where the 2'-amine is protonated.
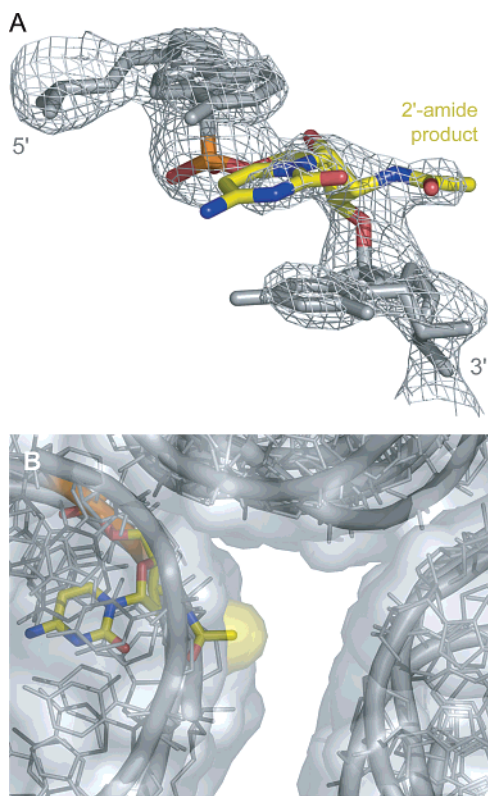
Figure 7. 2′-Amide product environment. (A) The 2′-amide product is accommodated without significant perturbation in an A-form helix. The 2′-amide nucleotide and flanking 5′ and 3′ residues are shown. Experimental electron density (gray mesh) is contoured at 1σ. (B) Large solvent channel in the vicinity of the 2′-amide crystal product. The in-crystal molecular envelope is represented as a gray surface and RNA backbones are shown as tubes.
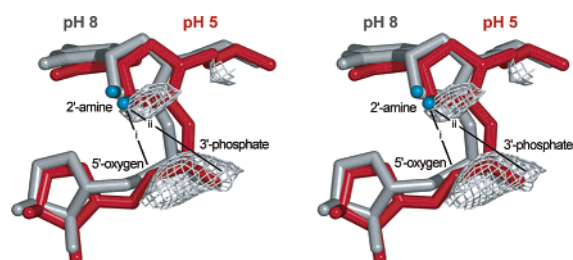
Figure 8. Structural consequences for 2′-amine protonation at position B6. Stereoimages are shown. Difference electron density (gray mesh) is calculated as $|F\mathrm{obs}_{pH5}| - |F\mathrm{obs}_{pH8}|$, is contoured at 2σ, and indicates regions in space selectively occupied at pH 5.

Atom movements associated with protonating the 2′-amine were characterized using difference electron density maps, $|F\mathrm{obs}_{pH5}| - |F\mathrm{obs}_{pH8}|$, drawn at the 2.0σ level (Figure 8). Comparison of the three unique 2′-amine groups present in the refined structure obtained at pH 5.2 revealed only a single site with a significant change in local structure relative to the pH 8.0 reference structure, at position B6 (Figure 8). This is the same nucleotide that yielded a 2′-amide product in the in-crystal acylation experiments, suggesting this position is relatively flexible in the crystal.

At position B6, we were able to observe, with confidence, local changes at the 2′-amine substituted nucleotide. Difference density is clearly seen in proximity to the 2′-amine, at the 5′-oxygen for the 3′-nucleotide, and at the nonbridging pro-S 3′-phosphate oxygen. There are two significant atom group movements. The largest movement is associated with the 3′-

phosphodiester group, which moves toward the 2′-amine (compare red, pH 5, and gray, pH 8, structures in Figure 8). This movement is accompanied by a small rotation of the nucleotide into the minor groove.

These conformational changes create two new local interactions with the potential to stabilize the 2′-amine acylation transition state. First, the 2′-amine is now within hydrogen bonding distance of the, strongly polar, bridging 5′-oxygen of the following nucleotide (distance *i* in Figure 8 changes from 4.0 to 3.1 Å). Second, the distance between the 2′-amine and the pro-S nonbridging oxygen anion decreases from 5.0 to 4.5 Å (distance *ii* in Figure 8).

Discussion

2′-Amine Substitutions in Duplex RNA: A Thermodynamic but Not Structural Perturbation. This work shows that 2′-amine groups in duplex RNAs do not perturb overall RNA duplex structure significantly (Figure 4) and therefore validate the widespread assumption that this substitution is a good structural probe for interactions at the 2′-ribose position. Because the 2′-amide product is also nonperturbing (Figure 7), amine-based chemistry is an ideal approach for site-selectively derivatizing RNA with fluorescent, cross-linking and other groups in structural and biophysical studies.

At a mismatched base pair or within an RNA loop, the thermodynamic consequences of a 2′-amine substitution vary from being moderately stabilizing to moderately destabilizing.[3,14] In contrast, introduction of a 2′-amine into an RNA duplex at a canonical base pair destabilizes a duplex by 1.2−1.4 kcal/mol.[5,14,17] The protonated 2′-NH_3^+ group incurs an additional unfavorable increment relative to the unprotonated form and destabilizes an RNA duplex by ∼2.1 kcal/mol.[5] These destabilizing thermodynamic effects for RNA hybridization could be due, in principle, either to structural *destabilization* of the final duplex structure or, alternately, *stabilization* of the single stranded, starting state.

Our crystallographic studies emphasize that substitution with a 2′-amine (Figures 3 and 4) or 2′-NH_3^+ (Figure 8) has either an undetectable or a very modest (at only one of three examples for the 2′-NH_3^+) effect on local nucleotide structure. The 2′-amine substitution is thus structurally, but not thermodynamically, conservative. We infer that 2′-NH_2 and 2′-NH_3^+ groups incur a thermodynamic cost for duplex stability, not by affecting the duplex stability per se, but by stabilizing conformations preferentially accessible in single-stranded states. The preferential stabilization of the single-stranded state may stem from the better ability of the more basic amine to form, possibly multidentate, hydrogen bonds with the 3′-nonbridging phosphate diester oxygens or with the bridging 5′-oxygen of the 3′-nucleotide (Figure 8).

A Trajectory for Phosphate Diester Catalysis of 2′-Amine Acylation.[21] We have visualized directly three states relevant to the trajectory for structure-sensitive 2′-amine acylation at flexible nucleotides. First, we have visualized the 2′-amine ground state in the C^N−A duplex (pH 8) structure (left-hand structure in Figure 9). Second, we have obtained the structure for the 2′-amide product, also at a mispaired nucleotide, by in-crystal acylation (right-most structure, Figure 9). Third, we visualized an approximate conformation for the 2′-amine, in a transition state-like conformation, in the C^N−A duplex at pH 5.
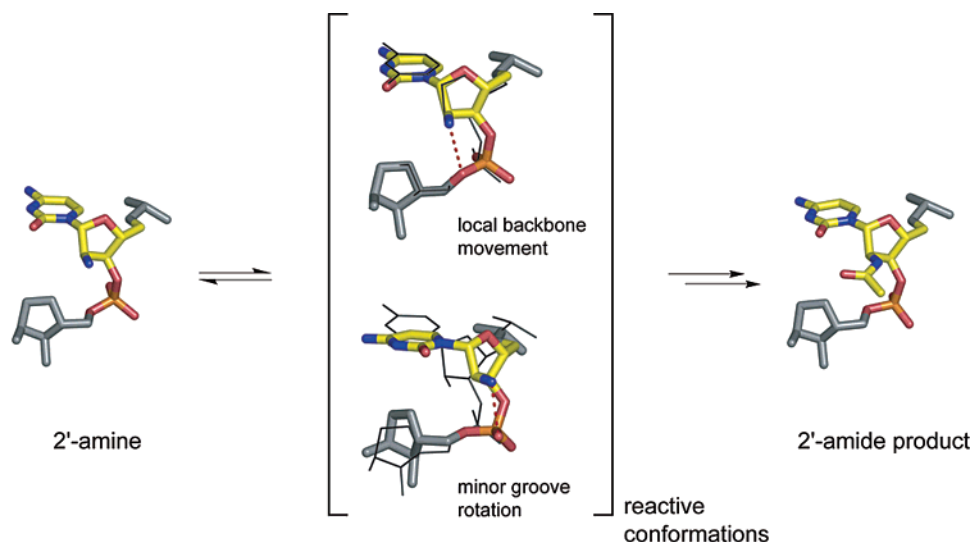
Figure 9. A molecular trajectory for 2′-amine acylation.[21] The C^N−A duplex (pH 8) and the 2′-amide in-crystal product structures are shown as the starting and final states, respectively. Favorable conformations for catalysis of 2′-amine acylation are shown in brackets. The local backbone movement structure was visualized as the C^N−A duplex at pH 5 and the minor groove rotation structure is adapted from a prior analysis[24] of RNA base flipping. For the center structures, thin black bonds indicate the nucleotide conformation in the 2′-amine ground state. Red dashed lines indicate strong (≤3 Å) electrostatic interactions.

The nucleotide that changed conformation upon protonating the amine at pH 5 is the same as the nucleotide that formed the 2′-amide product in our crystals. We infer that, in the context of the crystal, the B6 nucleotide is the one most able to adopt the alternate conformation required to facilitate 2′-amine acylation. One plausible trajectory for facilitated 2′-amine acylation thus involves a local change in backbone conformation at the 3′-phosphodiester group and movement of the 5′-oxygen to within 3 Å of the nucleophilic amine (see red dashed line, upper reactive conformation in Figure 9).

In addition to the transition state-like structure visualized crystallographically at pH 5, solution-phase experiments support the interpretation that the optimum conformation for 2′-amine acylation involves a movement in which the base flips out of the helix. This base flipping mechanism is supported by experiments showing that (*i*) 2′-amine acylation is most efficient when a nucleotide is unconstrained by base pairing or tertiary interactions[14−16] and (*ii*) for mismatched nucleotides, the efficiency of 2′-amine acylation is correlated with the number and quality of hydrogen bonds at the base moiety of a 2′-amine substituted nucleotide.[14]

In principle, base movement could occur toward either the minor or the major groove. However, both simple molecular models (data not shown) and energy minimization studies[24] indicate that, when an RNA base moves into the major groove, the 2′-amine is pulled into the helix and behind the ribose ring of the 3′ nucleotide, rendering the amine sterically inaccessible for acylation. In contrast, modeling studies (Figure 9) and energy minimization approaches[24] indicate that base movement into the minor groove readily yields conformations in which the 2′-ribose position lies close to the pro-S nonbridging oxygen of the adjacent 3′ phosphodiester group (see red dashed line, lower conformation in center of Figure 9).

We therefore propose that 2′-amine acylation can proceed via either of two facilitated transition states (Figure 9) whose relative contribution reflects the extent to which the state lowers the chemical barrier for acylation, as modulated by the frequency

with which the nucleotide reaches each state[21] (see movie in the Supporting Information). The transition state involving base rotation into the minor groove will lower the activation barrier for 2′-amine acylation by a greater extent due to the better ability of the more electronegative nonbridging oxygen to stabilize the partial charge on nitrogen in the transition state. Both canonically paired and mismatched nucleotides can likely react via the facilitated transition state that involves only the local backbone movement; whereas, conformationally flexible mismatched and unpaired nucleotides will be better able to reach the transition state conformation that requires base rotation into the minor groove (Figure 9). Both transition states share the requirement for proper positioning of the adjacent 3′-phosphodiester relative to the 2′-amine nucleophile.

Experimental Section

RNA Oligonucleotides, Crystallization, and Data Collection. Oligoribonucleotides (Trilink or Dharmacon) were based on a previously crystallized sequence[22] and form 16 base pair duplexes containing either C^N−A mismatches or C^N−G base pairs, where C^N indicates a 2′-amino cytidine nucleoside (Figure 2). Oligonucleotides were purified by denaturing gel electrophoresis [20% (w/v) polyacrylamide, 90 mM Tris-borate, 1 mM EDTA, 7 M urea] and recovered by electroelution. Crystallization experiments were performed at ambient temperature using the sitting drop vapor diffusion method. Initial solubility screens employed a sparse matrix approach[25] (Hampton Research). Equitriangular prisms (100−150 μm on a side) were observed in 2−3 days from drops containing equal volumes of 0.3 mM RNA and one of several crystallization conditions (Table 1), equilibrated against 35% (v/v) MPD in the reservoir. Intensity data were collected at 100 K using an in-house source and R-axis IV++ imaging system and processed using HKL.[26] All duplex crystals proved to be isomorphous and were solved in the $P3_121$ space group (Table 1A).

Structure Solution and Refinement. The structure of the C^N−A Duplex (pH 8.0) was solved by a combination of molecular replacement[27] and single isomorphous replacement.[28] A 16 base pair RNA

(24) Giudice, E.; Lavery, R. *J. Am. Chem. Soc.* **2003**, *125*, 4998−4999.

(25) Berger, I.; Kang, C.; Sinha, N.; Wolters, M.; Rich, A. *Acta Crystallogr.* **1996**, *D52*, 465−468.
(26) Otwinowski, Z.; Minor, W. *Methods Enzymol.* **1997**, *276*, 307−326.
(27) Navaza, J. *Acta Crystallogr.* **1994**, *50*, 157−163.

duplex with an identical sequence (PDB accession 405D)[22] was used as the search model. We were able to identify multiple independent duplexes in the unit cell by initially including a partial solution with relatively poor statistics (correlation coefficient 54.9% and R-factor 56.3%), but positioned on the 3-fold crystallographic *c*-axis, in a second round of molecular replacement. Identification of a second duplex solution inside the unit cell improved the correlation coefficient to 84.6% and the *R*-factor to 33.4%. Visualization of this solution in O,[29] in the context of crystallographic symmetry partners, showed that the duplex lying on the *c*-axis overlapped itself. Removing one strand of this duplex yielded a self-consistent unit cell containing 9 complete duplexes, with one full duplex and one single strand in the asymmetric unit. Refinement was performed using CNS,[28] with custom parameter and linkage constraints for the 2′-NH₂ ribose substitution. 5% of the reflections were reserved for cross-validation using R-free. After an initial rigid body refinement using data to 3.0 Å, R-cryst was 34.5% and R-free was 48.4%. At this stage, electron density maps showed that the molecular replacement solution was partially correct but that the full duplex was out of register. Phases from this solution were used to compute a difference map for a duplex with 5-iodouridine at position 3. Iodine positions visualized at 3σ indicated that the duplex needed to be shifted by two base pairs. Subsequent refinement by simulated annealing yielded R-cryst and R-free of 30.8% and 39%, respectively. Cycles of individual *B* factor refinement and energy minimization were performed against a maximum likelihood target using amplitudes; ions and water molecules were added; and refinement was continued until no further improvement was observed. Because all data sets were shifted to the same reference origin, subsequent structures could be refined directly using the C^N–A Duplex (pH 8.0) coordinates as the starting model. Refinement statistics are summarized in Table 1B.

In−Crystal Acylation and Structure Determination. To visualize the 2′-amine product, C^N−A duplex crystals [grown using a crystallization solution of 10% MPD, 50 mM Na-cacodylate (pH 8), 12 mM spermidine, 80 mM CaCl₂; 2 μL initial volume] were treated with 1 μL 250 mM sulfosuccinimidyl acetate (Pierce; Rₘ, Figure 1) in dimethyl sulfoxide. The reaction was stopped after 20 min by flash freezing the crystal in liquid nitrogen. After confirming the $P3_121$ space group, intensity data were shifted to the common origin and the structure was solved by refining against the C^N−A duplex coordinates. Initial simple $|F_o| - |F_c|$ difference maps, visualized at 2.5σ, indicated that the 2′-amide product formed at one of the three 2′-amine groups in the asymmetric unit (B6, see Figure 3). These maps were used to manually add the product atoms for refinement (Table 1). Product structures were analyzed using simulated annealing omit maps,[28] in which the entire 2′-amine substituted residue was excluded. When the simulated annealing maps are visualized at different sigma levels, the density for the cytidine base disappears at roughly the same rate as for the amide atoms, supporting the presence and correct position of the product atoms. The C^N (2′-amine-cytidine-5′-monophosphate) and product [2′-(*N*-acetamide)-cytidine-5′-monophosphate] nucleotides have been added to the PDB Chemical Component Dictionary under the codes [A5M] and [M5M], respectively. Coordinates for the C^N−A and C^N−G duplexes at pH 8, a C^N−A duplex at pH 5, the C^N−A product duplex, and a C−A control duplex have been deposited with the PDB (see Table 1 for accession codes). All structure figures and the movie in the Supporting Information were composed using PyMOL.[30]

Solution Phase 2′-Amine Acylation. 2′-amine acylation reactions were performed using 1 μM of 5′-[³²P]-labeled oligonucleotide and 75 mM sulfosuccinimidyl-6-(biotinamido)-hexanoate (Pierce; R_b, see Figure 1) at 37 °C and quenched using dithiothreitol (DTT). Reaction products were resolved by electrophoresis in 20% denaturing polyacrylamide gels and band intensities were quantified using a Phosphorimager (Molecular Dynamics). The pseudo-first-order acylation rate (k_{acyl}) was obtained by fitting to: fraction acylated product $= 1 - \exp(k_{acyl}/k_{hydrolysis}(e^{-k_{hydrolysis}t} - 1))$, where $k_{hydrolysis}$ is the rate of reagent hydrolysis.

Supporting Information Available: Movie (in QuickTime format) illustrating plausible trajectories for the 2′-amine acylation reaction. This material is available free of charge via the Internet at http://pubs.acs.org.

JA053647Y

(28) Brunger, A.; Adams, P.; Clore, G.; Delano, W.; Gros, P.; Grosse-Kunstleve, R.; Jiang, J.-S.; Kuszewski, J.; Nilges, M.; Pannu, N.; Read, R.; Rice, L.; Simonson, T.; Warren, G. *Acta Crystallogr. D54*, 905−921.
(29) Jones, T.; Zou, J.; Cowan, S.; Kjeldgaard, M. *Acta Crystallogr.* **1991**, *A47*, 110−119.
(30) DeLano, W. L. *The PyMOL Molecular Graphics System.*